AIChE

Hot Zones Formation During Regeneration of Diesel Particulate Filters

Kai Chen, Karen S. Martirosyan, and Dan Luss
Dept. of Chemical and Biomolecular Engineering, University of Houston, Houston, TX 77024

DOI 10.1002/aic.12266
Published online May 20, 2010 in Wiley Online Library (wileyonlinelibrary.com).

A diesel particulate filter (DPF) is used to remove particulate matter (PM) from the diesel engine exhaust. The accumulated PM is periodically removed by combustion, which sometimes leads to excessive temperature excursions that melt the ceramic filter. This behavior cannot be explained by operation under stationary feed conditions. We propose that these temperature excursions are a dynamic effect following a rapid change in the driving mode while the DPF is being regenerated. Specifically, a rapid decrease in the exhaust temperature can lead to a counterintuitive large transient temperature rise above that which would exist under a higher stationary feed temperature. This unexpected behavior is similar to the well-known wrong-way behavior in packed-bed reactors, even though the axial-dependent flow through the filter in a DPF is rather different from the constant axial flow through a packed bed. We present simulations that provide insight about the dependence of the amplitude of this wrong-way temperature rise on the filtration velocity, the PM loading, dimensions of the DPF, and the amplitude of the rapid temperature decrease and when it occurs after the start of the regeneration. The insight provided by these simulations will help develop operation and control protocols that circumvent or at least decrease the probability of the occurrence of the destructive melting of the DPF. © 2010 American Institute of Chemical Engineers *AIChE J,* 57: 497–506, 2011
Keywords: diesel particulate filter, temperature excursion, wrong-way behavior

Introduction

Diesel-driven cars have a higher efficiency and longer durability than gasoline-driven engines. Moreover, diesel engines have a lower emission of ''greenhouse gas'' (both CO_2 and NO_x) and hydrocarbons and enable a better cold start and safer fuel handling. Their main drawback relative to gasoline engines is about 10 times higher emissions of particulate matter (PM) of toxic organic compounds and heavy metals in the form of either solid particles or liquid droplets. The EPA issued strict limits on PM emission that are classified as carcinogenic materials and chemical smog components. A diesel particulate filter (DPF) is currently the most efficient device for reducing the PM emission. It is a ceramic block of thousands of square parallel porous channels, with the opposite end of adjacent channels being plugged. The exhaust gas flows through the porous walls from the inlet to the outlet channels, while about 95% of the PM accumulates on the filter.[1] The collected PM is periodically removed by combustion. The exothermic combustion leads in some cases to unexpected temperature excursions, which melt the common cordierite ceramic filter. The development of a safe and reliable regeneration procedure that circumvents the melting of the filter is the most demanding technological challenge in the operation of a DPF.

Extensive experiments[2–10] and theoretical simulations[11–26] attempted to determine what generates these large temperature excursions. Most studies determined the dependence of

Correspondence concerning this article should be addressed to D. Luss at dluss@uh.edu.

© 2010 American Institute of Chemical Engineers

the temperature rise on various operating conditions such as feed composition, temperature and flow rate, and PM-deposit layer thickness under stationary feed conditions. The temperature rise predicted by these studies is not sufficiently high to explain the observed melting of the DPF. It is well known that in packed-bed reactors the difference in the propagation speeds of the concentration and temperature perturbations can lead to a wrong-way behavior, i.e., a sudden decrease in the feed temperature below the bed temperature can cause a counterintuitive transient increase in the bed temperature above that existing before that perturbation.[27–35] This suggests that the melting occurs during the dynamic operation of the DPF, i.e., following a change in the car-driving mode such as a rapid shift from full-speed driving to idle during the DPF regeneration. Such a shift in the engine load decreases the exhaust temperature from about 900 to 600 K, increases the oxygen content in the exhaust gas from about 7 to 15%, and decreases the gas filtration velocity by a factor of 6.[18,36,37] It is essential to gain an understanding and ability to predict the magnitude of the temporal temperature rise as a function of sudden changes in the properties of the exhaust feed during the DPF regeneration. We have recently conducted experiments, which confirmed the conjecture that a sudden change in the DPF feed temperature can lead to a counterintuitive temperature rise.[38] We report here simulations and predictions of the dependence of this temperature rise on a rapid change in the DPF feed temperature. This information is essential for gaining an understanding of the impact of simultaneous changes in the exhaust temperature, oxygen concentration, and filtration velocity, which will be the subject of a forthcoming publication.

Development of the Mathematical Model

We describe the DPF by a one-dimensional model that assumes uniform distribution of the PM along the square channels. It does not account for wall heat losses, for differences among cells located at different radial positions and potential flow maldistribution among the channels. A schematic of single inlet and outlet channels separated by a filter of thickness w_s is shown in Figure 1. A soot layer of thickness w is deposited uniformly on the four walls of the inlet channel.

Previous studies illustrated that the temperature in the thin soot and filter layer were essentially uniform at any axial (z) location in the channel.[39] Because of the small thickness of the soot deposit, we ignore the change in flow area in the inlet channel upon combustion of the PM. The gas response is fast as its time constant is much shorter than that of the solid temperature. Thus, we used a quasi steady-state model to describe the gas phase in the inlet and outlet channels of the DPF. The mass, laminar flow momentum balances, and energy balances of the exhaust gas in the inlet ($i = 1$) and outlet channel ($i = 2$) are as follows:

$$\frac{\partial(d_i^2 \rho_i v_i)}{\partial z} = (-1)^i 4 d \rho_w v_w \tag{1}$$

$$\frac{\partial p_i}{\partial z} + \frac{\partial}{\partial z}(\rho_i v_i^2) = -\alpha_1 \mu(T_i) v_i / d^2 \tag{2}$$

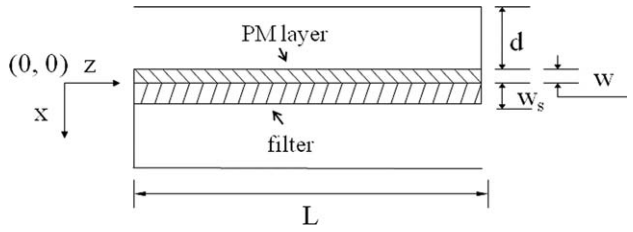

Figure 1. A schematic diagram of a pair of inlet and outlet channels.

$$C_{pg}(T_1)\rho_1 v_1 \frac{\partial T_1}{\partial z} = \frac{4}{d} h_1 (T_s - T_i) \tag{3a}$$

$$C_{pg}(T_2)\rho_2 v_2 \frac{\partial T_2}{\partial z} = (4/d)[h_2 + C_{pg}(T_2)\rho_w v_w](T_s - T_2). \tag{3b}$$

The pressure difference across the soot layer and ceramic wall satisfies the Darcy law

$$p_1 - p_2 = \frac{\mu(T) v_w}{k_s} w_s + \frac{\mu(T) v_w}{k_p} w. \tag{4}$$

The ideal gas law was used to calculate its density. As the pressure changes are very small, we calculated the gas density under atmospheric pressure. The other gas properties were calculated using the empirical relations reported in Bissett's article assuming that they are independent of temperature. The soot permeability was determined by the Pulkrabek and Ibele predictions.[40] Bissett and Shadman[41] showed that the length scale over which the gas temperature reached the same temperature as the solid temperature was several orders of magnitude smaller than the typical PM layer thickness. Thus, we assumed that the gas and solid temperature were equal in the PM layer. The energy balance of the solid phase is

$$\begin{aligned} \frac{\partial}{\partial t}(\rho_p w C_{pp}(T_s) T_s + \rho_s w_s C_{ps}(T_s) T_s) &= -h_1 (T_s - T_1) \\ &\quad - h_2 (T_s - T_2) + \Delta H \times \int_0^w R_{soot} dx \\ &\quad + \lambda_p \frac{\partial}{\partial z}\left(w \frac{\partial T_s}{\partial z}\right) + \lambda_s w_s \frac{\partial^2 T_s}{\partial z^2} + C_{pg} v_w \rho_w (T_1 - T_s), \end{aligned} \tag{5}$$

where the effective PM and filter conductivity accounts for those of both the gas and solid, i.e.,

$$\begin{aligned} \lambda_p &= \varepsilon \lambda_{gas} + (1 - \varepsilon)\lambda_{soot} \\ \lambda_s &= \varepsilon \lambda_{gas} + (1 - \varepsilon)\lambda_{wall}. \end{aligned} \tag{6}$$

The heat transfer coefficients h_1 and h_2 were assumed to be equal and were determined by the Shah and London prediction.[42] We used in all the simulations $h_1 = h_2 = 160$ W/(m^2 K), except when otherwise stated.

The corresponding channel front and end boundary conditions are

$$T_1 = T_{inlet1}; v_1 = v_{inlet}; T_2 = T_s; v_2 = 0; \frac{\partial T_s}{\partial z} = 0 \quad \text{at} \quad z = 0 \tag{7}$$

$$v_1 = 0; P_2 = P_{\text{atm}}; \frac{\partial T_s}{\partial z} = 0; \quad \text{at} \quad z = L. \tag{8}$$

We assume that the wall temperature is initially constant

$$T_s(0, z) = T_{\text{ini}}. \tag{9}$$

After the soot is ignited and a temperature front has formed, the feed temperature T_1 is step changed to a new temperature T_{new} at a specified time t.

The soot oxidation reactions are

$$C + \alpha O_2 \rightarrow 2(\alpha - 0.5)CO_2 + 2(1 - \alpha)CO, \tag{10}$$

where α is the oxidation reaction index, with values between 0.5 and 1. Reported α value for PM combustion is between 0.55 and 0.9.[43] We assume that $\alpha = 0.75$. The corresponding heat release is

$$\Delta H = 2(\alpha - 0.5)\Delta H_{CO_2} + 2(1 - \alpha)\Delta H_{CO}. \tag{11}$$

The reaction rate of the soot layer is

$$R_{\text{soot}} = \frac{S_p k_{ox}(T_s)\rho_p y}{M_c} \tag{12}$$

$$k_{ox}(T_s) = k_0 T_s \exp(-\frac{E}{RT_s}). \tag{13}$$

The reported apparent activation energy E is in the range of 80,000–160,000 J/mol. Our simulations were conducted with the value of 150,000 J/mol. The preexponential factor k_0 in the reaction rate expression was chosen as 6.0 m/(s K).[43]

The soot thickness during the regeneration satisfies the relation

$$\rho_p \frac{dw}{dt} = -M_c R_{\text{soot}}. \tag{14}$$

We assume that the soot is deposited uniformly on the surface.

$$w(0, z) = w_{\text{int}}. \tag{15}$$

The oxygen mole fraction in the PM and filter is computed by

$$\begin{aligned} v_w \frac{\partial y}{\partial x} - D_a - \frac{\partial}{\partial x}(\frac{\partial y}{\partial x}) &= \frac{M_c}{\rho_p} R_{\text{soot}} \\ v_w \frac{\partial y_s}{\partial x} - D_a \frac{\partial}{\partial x}(\frac{\partial y_s}{\partial x}) &= 0. \end{aligned} \tag{16}$$

The dispersion coefficient in the porous media was calculated by the empirical relation proposed by Delgado[44] and Yan[45]

$$D_a = \varepsilon D_m + 0.5 d_p u, \tag{17}$$

where u is the gas filtration velocity, ε is porous media porosity, and d_p the diameter of PM particles.

The corresponding boundary conditions are

$$v_w y_{-w} - D_a - \frac{\partial y}{\partial x}|_{x=-w} = v_w y_1 - k_1(y_{-w} - y_1) \tag{18}$$

Table 1. Geometry and Thermophysical Properties of the DPF and Soot Deposit Used in the Simulations

Filter material	Cordierite
DPF length	150 mm
Channel width	1.0 mm
Filter thickness	0.40 mm
Bulk density of filter	1400 kg/m^3
Permeability of clean filter	1×10^{-12} m^2
Porosity of filter	60%
Mean pore size of clean porous wall	25 μm
Bulk density of soot deposit	160 kg/m^3
Permeability of soot deposit	1×10^{-14} m^2
Porosity of soot deposit	60%

$$-D_a \frac{\partial y}{\partial x}|_{w_s} = k_2(y_{w_s} - y_2). \tag{19}$$

The mass transfer coefficient k_i for the inlet and outlet channels was computed by the relation

$$k_i = \frac{Sh \times D}{d_i}. \tag{20}$$

The Hayes and Kolaczkowski equation[46,47]

$$Sh = 3.66(1 + 0.095 \frac{d_i}{L} Pe)^{0.45} \tag{21}$$

is used to determine the Sherwood number for the laminar flow in the square channels.

Numerical simulations were conducted for a DPF with a uniform initial PM layer of thickness w_{ini} and initial temperature of $T_{\text{ini.}}$ The set of differential equations 1–4 and the corresponding boundary conditions were solved by the shooting method. The solution of the system equations determined the channel flow field, the pressure field, and the gas temperature field. The transient differential equation 5 was solved by an implicit finite difference method in space using 40 grid points in the axial direction. An implicit solution in time with a time step of 0.1 s was used to avoid the numerical instabilities. The properties of the DPF used in the simulations are reported in Table 1.

Wrong-Way Behavior in a DPF

Numerical simulations were conducted to determine if and how a sudden decrease in the feed temperature while keeping all the other input variables unchanged may lead to a wrong-way behavior. All the simulations were conducted at a constant filtration velocity defined as the inlet flow rate divided by the filter area. The surface area of a channel with a cross-sectional area of 1×10^{-6} m^2 and 0.15 m long is 0.6×10^{-3} m^2. Hence, an inlet velocity of 15 m/s corresponds to a filtration velocity of 2.5 cm/s. Almost all the simulations, except when otherwise stated, were conducted for a PM loading of 10 g/L, an oxygen concentration of 10 vol %, and a filtration velocity of 2.5 cm/s. The axial temperature profiles shown in all the figures are of the solid (PM and filter) phase.

An initial set of simulations was conducted to determine the behavior under stationary feed conditions. These simulations

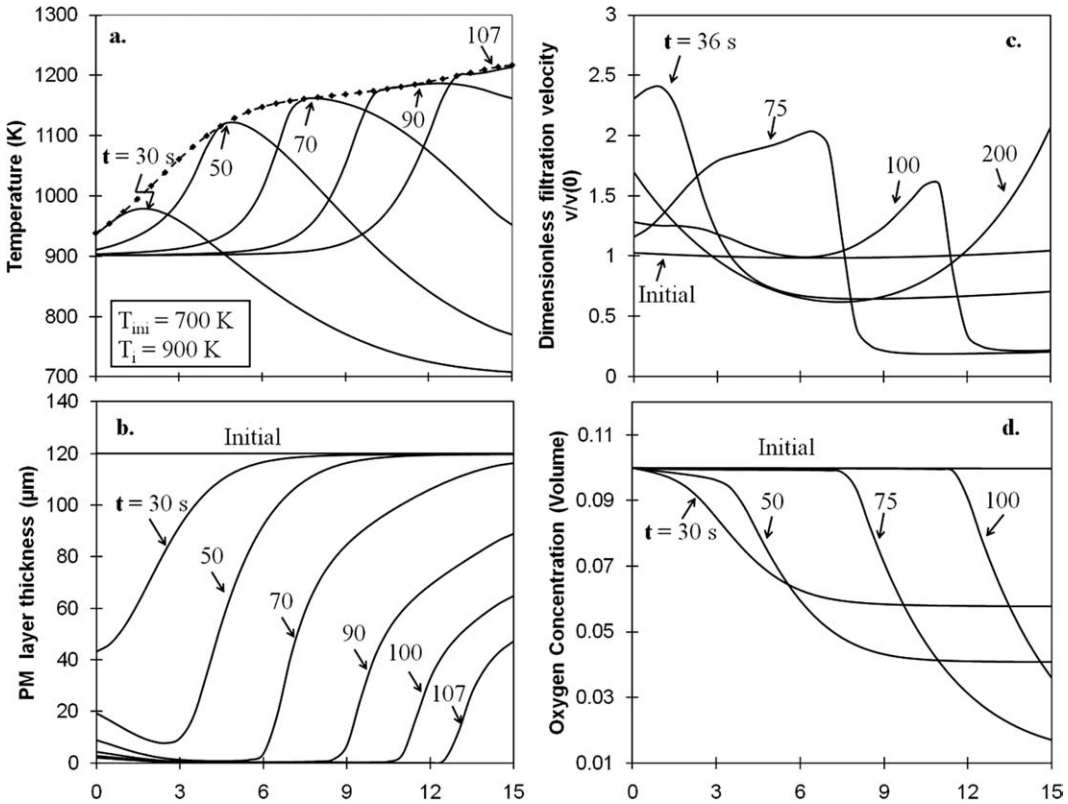

Figure 2. (a) Temporal axial temperature profiles during PM regeneration under stationary feed condition.

(b) Corresponding temporal deposited PM profiles. (c) Evolving dimensionless filtration velocity profiles where $v(0) = 2.5$ cm/s. (d) Profile of O_2 concentration in the inlet channel at selected time.

showed that when the feed temperature was sufficiently high to ignite the PM, a combustion wave formed and moved downstream regenerating the DPF. For example, Figure 2a describes the behavior of a DPF, which was initially at a uniform temperature of 700 K and was fed at $t = 0$ with exhaust gas having a stationary temperature of 900 K. The peak of the moving temperature wave increased as it moved downstream. The highest peak temperature was attained at the end of the DPF. The dashed-diamond line in this and all other figures describes the peak temperature obtained under stationary feed conditions.

Figure 2b shows the transient PM profiles corresponding to the case shown in Figure 2a. The regeneration consumed first the PM in the upstream section of the channel and then the downstream section. As the filtration velocity is a function of temperature and pressure, the corresponding evolving dimensionless filtration velocity profiles, shown in Figure 2c, are, as expected, rather strongly dependent on the local resistance to the flow, where we define the dimensionless filtration velocity as filtration velocity divided by the initial filtration velocity. Before the start of the regeneration, the filtration velocity is almost uniform along the DPF with a slight minimum in its center, too small to be visible in Figure 2c. As the regeneration consumed first the PM from the upstream of the inlet channel, the velocity profile attained a maximum in that section and a minimum in the nonregenerated downstream section. With time the location of the maximum velocity shifted downstream. After complete removal of the PM layer the velocity attained a minimum in the center of the DPF. This minimum is much more dominant than the one before the start of the regeneration as the resistance of the cordierite filter to the flow is much smaller (order of 100) than that of the PM layer. The calculated inlet oxygen concentration profiles along the filter during soot regeneration process are shown in Figure 2d. The model predicts that initially a significant decrease of the O_2 concentration occurs in the upstream section of the inlet channel in which the ignition started. Because of the large consumption of O_2 at the upstream section of the DPF the reaction rate in the downstream was limited by the oxygen availability. After the soot at the upstream was completely burned the temperature front propagated toward the downstream and higher oxygen supply became available for the soot combustion. This increased the reaction rate and the peak temperature.

The simulations revealed that a sudden decrease in the exhaust feed temperature below that of the solid phase can generate a counterintuitive transient increase in the temperature of the moving wave, i.e., a wrong-way behavior. Figure 3 shows cases in which a DPF with an initial temperature of 700 K was fed with an exhaust gas at a temperature of 900 K. This generated a downward moving temperature wave. After 75 s, the feed temperature was rapidly decreased to 700 K. This increased the moving wave temperature above the value it would have attained if the feed temperature would have remained constant at the higher value of 900 K. The amplitude of the wrong-way temperature wave rise in this case increased monotonically with distance from the feed inlet. For the case shown in Figure 3a, the wrong-way

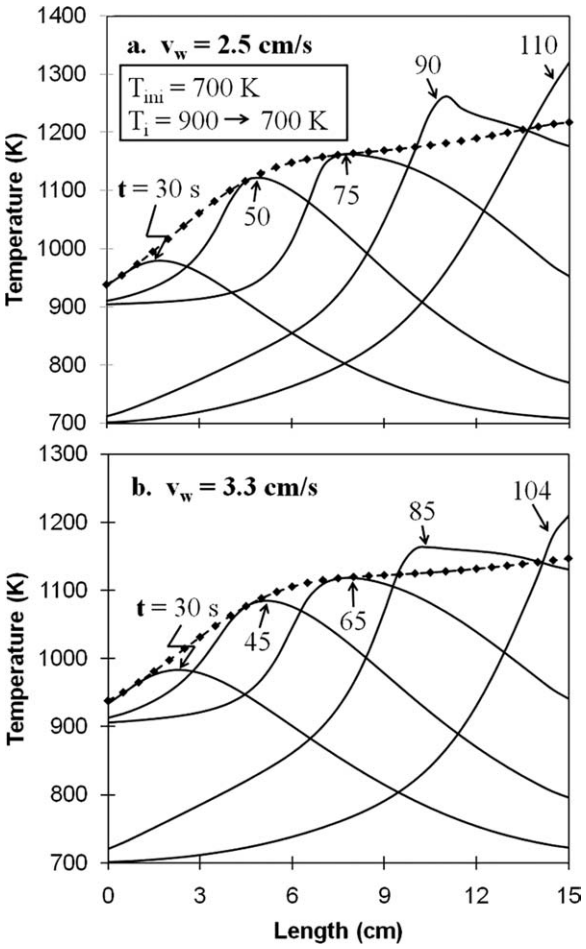

Figure 3. Impact of filtration velocity on temporal temperature profiles.

In both cases, temperature perturbation is initiated when temperature front reaches $x/L = 0.5$.

behavior led to a transient temperature rise of about 102 K at the DPF outlet.

The amplitude of the stationary temperature wave as well as of the wrong-way behavior depended on the filtration velocity. Although a higher filtration velocity increases the supply of the oxygen to the deposited PM and the velocity of the moving combustion wave, it also increases the rate of heat removal from the PM layer. At low and high filtration velocities an increase in the velocity increases the peak stationary temperatures as the dominant impact of the increased velocity is the increase in the oxygen supply and hence the reaction rate. However, at intermediate filtration velocities the heat removal rate becomes the dominant impact so that the peak temperature decreases upon an increase in the filtration velocity. The filtration feed velocity in Figure 3b was (3.3 cm/s) higher than that in Figure 3a (2.5 cm/s). In both cases, the feed temperature was rapidly changed from 900 to 700 K when the reaction wave was at about $x/L = 0.5$. A comparison of the temperature profiles of these two cases shows that increasing the filtration feed velocity decreased the peak temperature of the moving wave under stationary feed conditions and slightly shortened their sojourn in the DPF. It also decreased the amplitude of the wrong-way behavior following a sudden feed temperature decrease.

The intricate impact of the filtration velocity on both the peak temperature under stationary feed conditions and the wrong-way temperature rise is illustrated by Figure 4. When the feed velocities were increased from 0.83 to 4.17 cm/s, the largest peak temperature under stationary feed conditions and the largest wrong-way temperature rise were attained at two different intermediate filtration velocities. The largest peak temperature under stationary feed conditions (solid line in Figure 4) of 1374 K was attained at a filtration velocity of 1.67 cm/s. The maximum peak temperature decreased upon additional increase in the filtration velocity. Simulations, not shown here, indicated that if the combustion rate was higher by about an order of magnitude, the peak temperature attained a local minimum at high filtration velocities and increased at higher filtration velocities. For filtration velocities smaller than 1.67 cm/s a sudden decrease of the feed temperature did not effectively cool the DPF, and no wrong-way behavior occurred. The wrong-way temperature rise attained its maximum at filtration velocities higher than that at which the maximum peak temperature was attained. For the case shown in Figure 4, as the feed temperature was decreased from 900 to 700 K, the wrong-way temperature rise was 40 and 102 K for filtration velocities of 1.67 and 2.5 cm/s, respectively. At higher filtration velocities the amplitude of the wrong-way temperature rise decreased because of the increased rate of heat removal.

The predicted amplitude of the wrong-way behavior depended on both the amplitude of the sudden temperature decrease as well as when it was caused. Figure 5 describes cases in which the initial behavior is identical to that in Figure 3a. The amplitude of the wrong-way behavior was a monotonic increasing function of the amplitude of the sudden temperature decrease (Figure 5a). The amplitude of the wrong-way behavior depended on the location of the moving temperature when the feed temperature was decreased, as shown in Figure 5b. In this example, the maximum temperature rise at the reactor exit following a temperature decrease

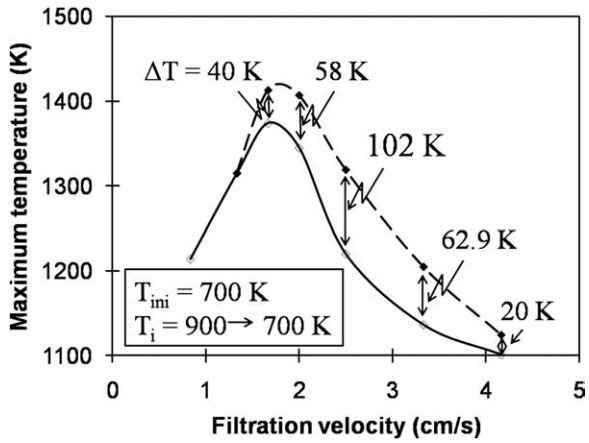

Figure 4. Impact of the feed velocity on the peak temperature under stationary feed conditions (solid line) and following a rapid temperature decrease when the temperature front reaches $x/L = 0.5$ (dashed line).

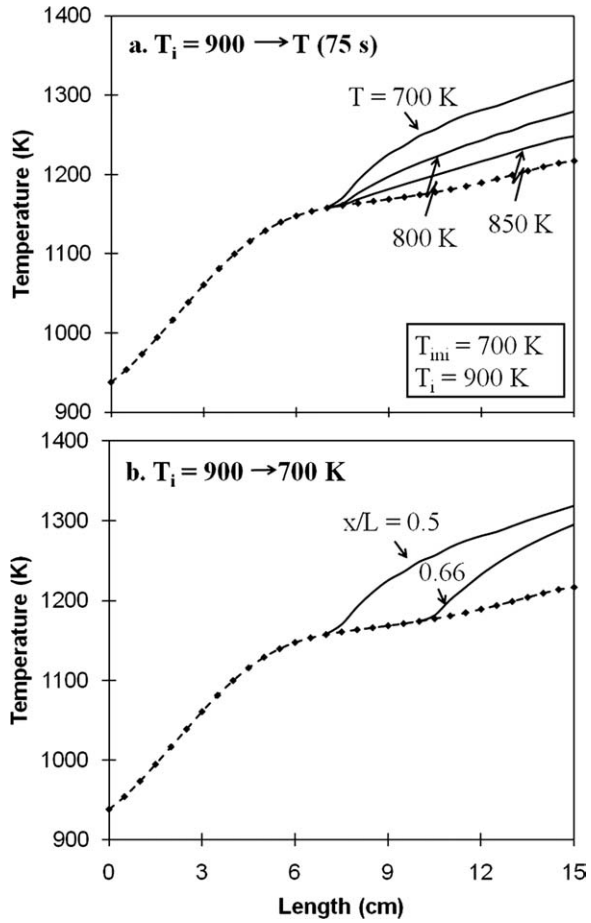

Figure 5. Dependence of the amplitude of the wrong-way temperature rise on (a) the amplitude of the sudden temperature decrease and (b) the position of the temperature front when the feed temperature is decreased.

when the temperature front was at $x/L = 0.5$ was higher than that when it was at $x/L = 0.66$.

The simulations showed that under fixed filtration velocity the temperature at the end of the inlet channel slightly increased with the length of the DPF (Figure 6b). However, the peak temperature at the end of a DPF of length L was higher than that of the peak temperature at the center of a DPF of length $2L$, as illustrated by Figure 6a. This effect was due to the spatial variation in the PM layer thickness, filtration velocity, and the convective heat transfer in the DPF. The amplitude of the wrong-way behavior was a monotonic increasing function of the DPF length following a feed temperature decrease from 900 to 700 K when the moving front was at $x/L = 0.5$ as shown in Figure 6b. For example, the wrong-way temperature rise was 87 and 110 K in a DPF of 0.09 and 0.18 m long, respectively.

The initial DPF temperature affected the temperature and velocity of the moving reaction front under stationary feed conditions as well as the wrong-way temperature rise. Figure 7a describes a case in which the initial DPF temperature was 900 K and the feed temperature was rapidly decreased from 900 to 700 K at $t = 45$ s. A comparison of Figure 3a with Figure 7a shows that the increase in the initial DPF temperature increased both the velocity and temperature of the moving temperature wave under stationary feed conditions. For example, the peak temperatures at the end of the feed channel were 1297.5 and 1242.9 K for the cases shown in Figures 7a and 3a, respectively. However, the wrong-way temperature rise was smaller for the higher initial DPF temperature. For example, the wrong-way temperature rise at the end of the feed channel of the DPF was 104 and 54 K for the case shown in Figures 3a ($T_{ini} = 700$ K) and 7a ($T_{ini} = 900$ K), respectively. The evolving PM profiles corresponding to the case shown in Figure 7a are shown in Figure 7b.

The initial PM loading affects both the peak moving wave temperature as well as the wrong-way temperature rise. Figure 8a shows the temperature profiles for a PM loading of 12 g/L somewhat higher than those in Figure 3a of 10g/L. A comparison of the two figures shows that the increase of the initial PM loading slightly increased the total regeneration time under stationary feed conditions (from 110 to 116 s) but increased the peak temperature at the end of the DPF by 3.9% from 1246 to 1294 K. However, the amplitude of the

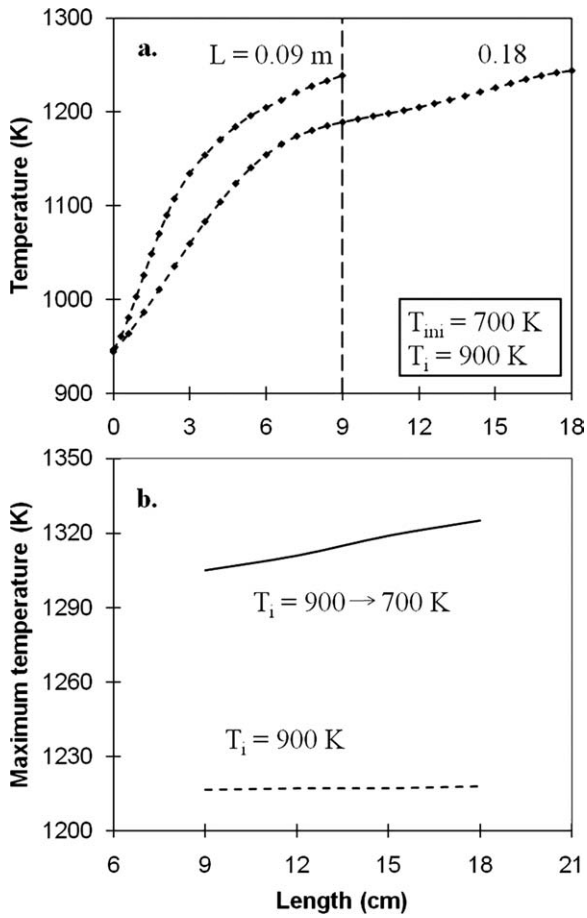

Figure 6. (a) Peak local temperature under stationary feed conditions for a DPF length of 0.09 and 0.18 m.

(b) Impact of DPF length on the maximum temperature under stationary feed conditions (dashed line) and following a sudden temperature decrease when temperature front reaches $x/L = 0.5$ (solid line).

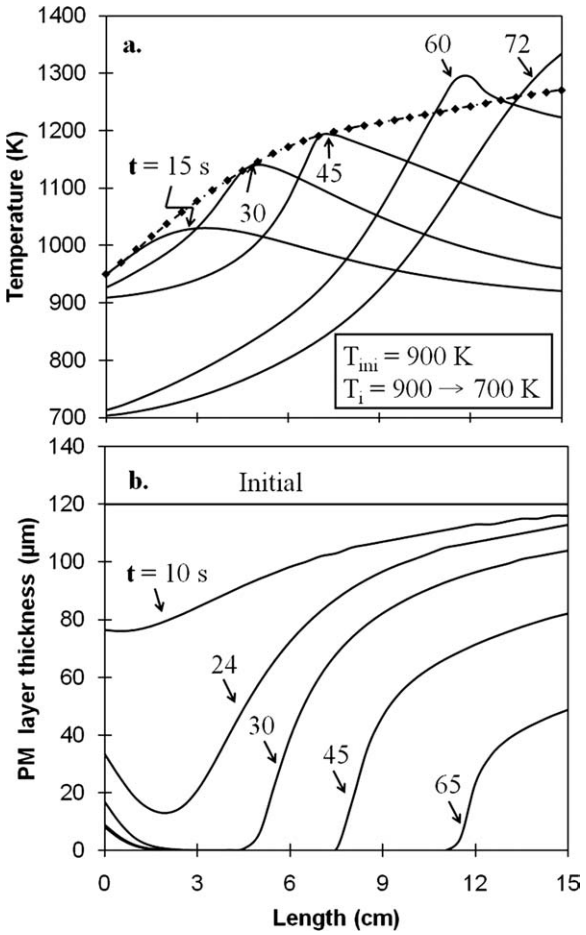

Figure 7. (a) Wrong-way behavior of PM combustion. Feed temperature is decreased at when front reaches $x/L = 0.5$.

(b) Corresponding transient PM-deposit thickness profile.

wrong-way temperature rise at the end of the DPF is more sensitive to changes in the PM loading. A comparison of the two figures shows that the increase of the PM loading from 10 to 12 g/L increased the amplitude by 36% from 104 to 141 K.

Figure 8b is of a case in which the filtration velocity was 3.3 cm/s the same as that in Figure 3b. Comparing the two figures shows that under stationary feed conditions the increase in the PM loading from 10 to 12 g/L increased the temperature at the DPF end by 4.4% from 1163 to 1214 K. However, the amplitude of the wrong-way temperature rise at the end of the DPF following a decrease of the feed temperature from 900 to 700 K increased by 29% from 62 to 80 K. Comparing Figure 8 parts a and b indicates that increasing the filtration velocity decreases the amplitude of the wrong-way behavior.

The heat transfer coefficient between the gas flowing in the inlet and outlet channels and the filter affects both the amplitude and velocity of the temperature fronts as well as the amplitude of the wrong-way temperature rise. Figure 9 compares the behavior for two values of the heat transfer coefficients ($h = 160$ and $h = 320$ W/(m^2 K)) before and after a decrease of the feed temperature from 900 to 700 K when the reaction wave reached $x/L = 0.5$. Figure 9a is for a case that the initial DPF temperature is 700 K, whereas that of Figure 9b is for an initial temperature of 900 K. In both cases, the higher value of the heat transfer coefficient generates sharper temperature fronts that move at a higher velocity through the DPF. The increase in the heat transfer coefficient also increases the amplitude of the wrong-way behavior. For example, it is 54 and 120 K for the two cases shown in Figure 9b.

Discussion and Concluding Remarks

The goal of our research was to gain an understanding and ability to predict the observed the reported unexpected melting of DPF. This understanding is essential for a rational development of operation and control protocols that circumvent or at least decrease the probability of this destructive event. Earlier studies have claimed that DPF overheating may occur because of decreased rate of heat removal following a sudden decrease of the flow rate or an increase of the oxygen concentration.[15,17,18] Our study indicates that it may

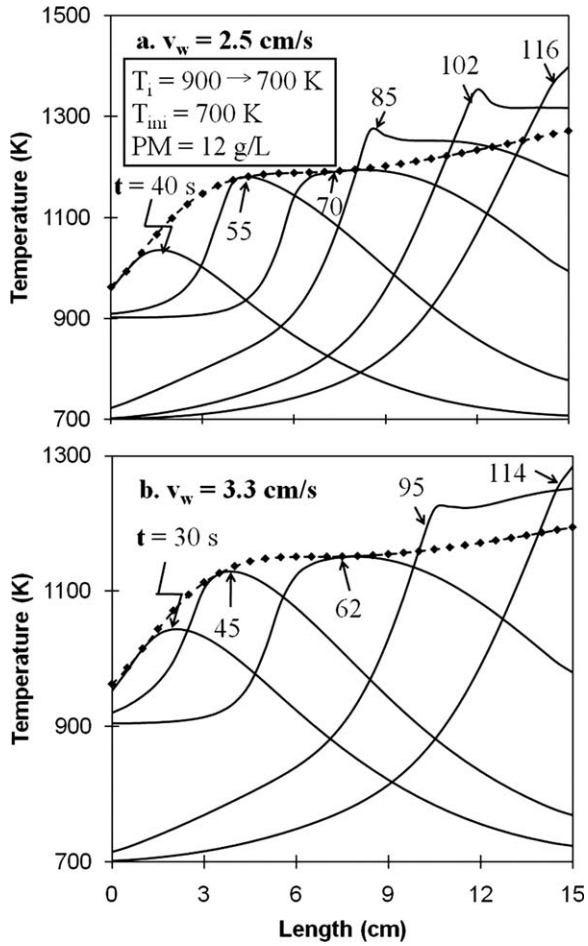

Figure 8. Impact of filtration velocity on wrong-way behavior during PM combustion.

PM loading of 12 g/L. Feed temperature is decreased when temperature front reaches $x/L = 0.5$.

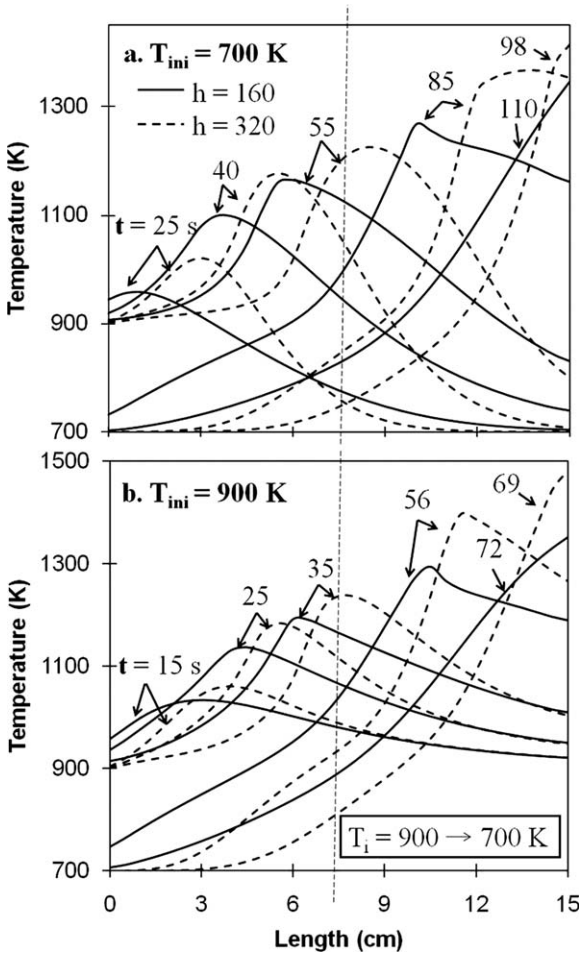

Figure 9. Impact of the heat transfer coefficient on the wrong-way behavior of PM combustion.

Initial DPF temperature is (a) 700 K and (b) 900 K. Solid line $h = 160$ W/(m^2 K); dashed line $h = 320$ W/(m^2 K). Temperature is decreased when front reached $x/L = 0.5$.

occur even when neither of these effects occur. The simulations show that a sudden decrease in the temperature of the exhaust feed to a DPF, while it is being regenerated, can lead to a transient counterintuitive increase in the DPF temperature, i.e., to a wrong-way behavior. Such a decrease in the exhaust temperature may be caused by a rapid shift from normal mode of driving to idle. Our recent experiments confirm this conjecture.[38] The simulations provide useful insight on the dependence of this wrong-way behavior on the various operating conditions and on when the temperature decrease occurs.

The wrong-way behavior in a DPF is rather different from that studied in adiabatic packed-bed reactors[27–35,48] or in a monolith convertors[49] in which the heat generated by the reaction is transported in the axial direction by convection and conduction. In the DPF, heat is transported through the filter walls by the convection of the gas. The filtration velocity affects both the heat removal and rate of heat generation in the deposited PM layer. The different dependence of these two rate processes on the filtration velocity is the cause of the nonmonotonic dependence of the temperature rise under stationary operation and of the wrong-way temperature rise on the filtration velocity. (Figure 4). The axial flow is essentially constant in packed-bed reactors and monolith converters but is a monotonically decreasing function of the distance in the inlet channels of a DPF. Thus, the existing criteria and predictions of the wrong-way behavior in packed-bed reactors cannot be readily modified to predict those in DPFs. It would be very useful to develop criteria predicting the behavior of a DPF similar to those available for an adiabatic packed-bed reactor. This modification will be rather difficult because of the intricate evolution of the filtering velocity profile along the DPF during the regeneration (Figure 2c).

The simulations predicted that the magnitude of the wrong-way behavior depended in a complex fashion on the initial bed temperature, amplitude of the temperature decrease and when it occurred, filtration velocity, and initial PM loading. In practice, the initial PM layer deposition is often not uniform along the DPF and often is not exactly known or can be accurately predicted. This complicates the rational development of a controlled regeneration procedure that circumvents the formation of the undesired local hot zones. We report here simulations of the impact of sudden changes in the exhaust temperature. As mentioned in the introduction, a shift in the driving mode usually causes simultaneous changes of the feed temperature, oxygen concentration, and filtration velocity. Each of these changes has a different impact on the DPF temperature. A future study will be concerned with the impact of these simultaneous perturbations and their interactions. This information is of particular interest as changes in velocity may also lead to wrong-way behavior.[18,50]

Acknowledgment

The authors thank the NSF for financial support of this research.

Notation

C_p = specific heat capacity, J/(kg K)
D = effective mass diffusivity, m^2/s
d = hydraulic diameter of clean channel, m
d_i = hydraulic diameter of channel i, m
d_p = mean pore size, m
E = activation energy, J/mol
h = convective heat transfer coefficient, W/(m^2 K)
ΔH_{CO} = specific heat of CO formation, J/mol
ΔH_{CO2} = specific heat of CO_2 formation, J/mol
k_i = mass transfer coefficient of O_2 in the channel i, m/s
k_o = reaction rate frequency factor
k_{ox} = reaction rate coefficient
k_p = permeability of soot deposit, m^2
k_s = permeability of ceramic filter, m^2
L = length of ceramic filter, m
M = molecular weight, kg/mol
Pe = Peclet number
P = exhaust gas pressure, Pa
R = gas constant, m^3 Pa/(mol K)
R_{soot} = reaction rate, mol/(m^3 s)
s_p = specific area of soot deposit layer, m^{-1}
Sh = Sherwood number
T = Temperature, K
t = time, s
v = velocity, m^2
w = thickness of soot deposit, m
w_s = thickness of ceramic filter wall, m

x = distance, m
y = oxygen concentration of the exhaust gas, mole fraction
z = axial distance, m

Greek letters

α = index for the completeness of thermal oxidation
α_1 = constant in channel pressure drop correlation
ΔH = reaction heat, J/mol
ΔP = backpressure, Pa
λ_p = soot deposit thermal conductivity, W/(m K)
λ_s = ceramic filter thermal conductivity, W/(m K)
ε = soot deposit porosity
μ = exhaust gas viscosity
ρ = density, kg/m^3

Subscripts

g = exhaust gas
i = channel index, 1 = inlet channel and 2 = outlet channel
p = particulate layer
s = substrate layer
w = wall-outlet channel interface

Literature Cited

1. Adler J. Ceramic diesel particulate filters. *Int J Appl Ceram Technol*. 2005;2:429–439.
2. Chen K, Martirosyan KS, Luss D. Soot combustion dynamics in a planar diesel particulate filter. *Ind Eng Chem Res*. 2009;48:3323–3330.
3. Hanamura K, Suzuki T, Tanaka T, Miyairi Y. Visualization of combustion phenomena in regeneration of diesel particulate filter. *Proc Soc Auto Eng 2003 World Congress*. Detroit, MI, SAE Paper No. 2003–01-0836, 2003.
4. Hayashi K, Ogura Y, Kobashi K, Sami H, Fukami A. Regeneration capability of wall-flow monolith diesel particulate filter with electric heater. Proc Soc Auto Eng 1990 World Congress. Detroit, MI, SAE Paper No. 900603, 1990.
5. Herz RK, Sinkevitch RM. Reactor for investigation of soot combustion on filter surfaces. *Carbon*. 1986;24:457–462.
6. Hoffmann U, Ma J. Study on regeneration of diesel particulate filter using a laboratory reactor. *Chem Eng Technol*. 1990;13:251–258.
7. Martirosyan KS, Chen K, Luss D. Behavior features of soot combustion in diesel particulate filter. *Chem Eng Sci*. 2010;65:42–46.
8. McCabe RW, Sinkevitch RM. A laboratory combustion study of diesel particulates containing metal additives. Proc Soc Auto Eng 1986 World Congress. Detroit, MI. SAE Paper No. 860011, 1986.
9. Montierth MR. Fuel additive effect upon diesel particulate filters. Proc Soc Auto Eng 1984 World Congress. Detroit, MI, SAE Paper No. 840072, 1984.
10. Schmidt N, Root T, Wirojsakunchai T, Schroeder E, Kolodziej C, Foster DE, Suga T, Kawai T. Detailed diesel exhaust particulate characterization and DPF regeneration behavior measurements for two different regeneration systems. Proc Soc Auto Eng 2007 World Congress. Detroit, MI, SAE Paper No. 2007–01-1063, 2007.
11. Aoki H, Asano A, Kurazono K, Kobashi K, Sami H. Numerical simulation model for the regeneration process of a wall-flow monolith diesel particulate filter. Proc Soc Auto Eng 1993 World Congress. Detroit, MI, SAE Paper No. 930364, 1993.
12. Bissett EJ. Mathematical model of the thermal regeneration of a wall-flow monolith diesel particulate filter. *Chem Eng Sci*. 1984;39:1233–1244.
13. Dardiotis CK, Haralampous OA, Koltsakis GC. Catalytic oxidation performance of wall-flow versus flow-through monoliths for diesel emissions control. *Ind Eng Chem Res*. 2006;45:3520–3530.
14. Guo Z, Zhang Z. Hybrid modeling and simulation of multidimensional processes for diesel particulate filter during loading and regeneration. *Numer Heat Transfer A*. 2007;51:519–539.
15. Haralampous OC, Koltsakis GC, Samaras ZC. Partial regenerations in diesel particulate filters. *Proc Soc Auto Eng 2003 World Congress*. Detroit, MI, SAE Paper No. 2003–01-1881, 2003.
16. Huynh CT, Johnson JH, Yang SL, Bagley ST, Warner JR. A One-dimensional computational model for studying the filtration and regeneration characteristics of a catalyzed wall-flow diesel particulate filter. *Proc Soc Auto Eng 2003 World Congress*. Detroit, MI, SAE Paper No. 2003–02-0841, 2003.
17. Koltsakis GC, Stamatelos AM. Modes of catalytic regeneration in diesel particulate filters. *Ind Eng Chem Res*. 1997;36:4155–4165.
18. Koltsakis GC, Haralampous OA, Samaras ZC, Kraemer L, Heimlich F, Behnk K. Control strategies for peak temperature limitation in DPF regeneration supported by validated modeling. *Proc Soc Auto Eng 2007 World Congress*. Detroit, MI. SAE Paper No. 2007–01-1127, 2007.
19. Konstandopoulos AG, Kostoglou M, Housiada P, Vlachos N, Zarvalis D. Multichannel simulation of soot oxidation in diesel particulate filters. *Proc Soc Auto Eng 2003 World Congress*. Detroit, MI, SAE Paper No. 2003–01-0839, 2003.
20. Miyairi Y, Miwa S, Abe F, Xu Z, Nakasuji Y. Numerical study on forced regeneration of wall-flow diesel particulate filters. *Proc Soc Auto Eng 2001 World Congress*. Detroit, MI, SAE Paper No. 2001–01-0912, 2001.
21. Optis CN, Johnson JH. A 2-D computational model describing the flow and filtration characteristics of a ceramic diesel particulate trap. *Proc Soc Auto Eng 1998 World Congress*. Detroit, MI, SAE Paper No. 980545, 1998.
22. Pontikakis G, Stamatelos A. Three-dimensional catalytic regeneration modeling of SiC diesel particulate filters. *J Eng Gas Turbines Power*. 2006;128:421–433.
23. Sbrizzai F, Faraldi P, Soldati A. Appraisal of three-dimensional numerical simulation for sub-micron particle deposition in a micro-porous ceramic filter. *Chem Eng Sci*. 2005;60:6551–6563.
24. Zheng H, Keith JM. New design for efficient diesel particulate trap regeneration. *AICHE J*. 2004;50:184–191.
25. Zheng H, Keith JM. Ignition analysis of wall-flow monolith diesel particulate filters. *Catal Today*. 2004;98:113–122.
26. Haralampous OA, Koltsakis GC. Oxygen diffusion modeling in diesel particulate filter regeneration. *AICHE J*. 2004;50:2008–2019.
27. Boreskov GK, Slinko MG. Modeling of chemical reactors. *Pure Appl Chem*. 1965;4:611–624.
28. Chen YC, Luss D. Wrong-way behavior of packed-bed reactors: influence of interphase transport. *AICHE J*. 1989;35:1148–1156.
29. Crider JE, Foss AS. Computational studies of transients in packed tubular chemical reactors. *AICHE J*. 1966;12:514–522.
30. Hoiberg JA, Lyche BC, Foss AS. Experimental evaluation of dynamic models for a fixed-bed catalytic reactor. *AICHE J*. 1971;17:1434–1447.
31. Mehta PS, Sams WN, Luss D. Wrong-way behavior of packed-bed reactors. I. The pseudo-homogeneous model. *AICHE J*. 1981;27:234–246.
32. Pinjala V, Chen YC, Luss D. Wrong-way behavior of packed-bed reactors. II. Impact of thermal dispersion. *AICHE J*. 1988;34:1663–1672.
33. Sharma CS, Hughes R. The behavior of an adiabatic fixed bed reactor for the oxidation of carbon monoxide. II. Effect of perturbations. *Chem Eng Sci*. 1979;34:625–634.
34. Van Doesburg H, DeJong WA. Transient behavior of an adiabatic fixed-bed methanator. I. Experiments with binary feeds of CO or CO_2 in hydrogen. *Chem Eng Sci*. 1976;31:45–51.
35. Van Doesburg H, DeJong WA. Transient behavior of an adiabatic fixed-bed methanator. II. Methanation of mixtures of carbon monoxide and carbon dioxide. *Chem Eng Sci*. 1976;31:53–58.
36. Johnson VT. Diesel emission control in reviews the Last 12 Months. *Proc Soc Auto Eng 2003 World Congress*. Detroit, MI, SAE Paper No. 2003–01-0039, 2003.
37. Setten BAAL, Makkee M, Moulijn JA. Science and technology of catalytic diesel particulate filters. *Catal Rev*. 2001;43:489–564.
38. Chen K, Martirosyan KS, Luss D. Wrong-way behavior of soot combustion in a planar diesel particulate filter. *Ind Eng Chem Res*. 2009;48:8451–8456.
39. Haralampous OA, Koltsakis GC. Intra-layer temperature gradients during regeneration of diesel particulate filters. *Chem Eng Sci*. 2002;57:2345–2355.
40. Pulkrabek WW, Ibele WE. The effect of temperature on the permeability of a porous material. *Int J Heat Mass Transfer*. 1987;30:1103–1109.
41. Bissett EJ, Shadman F. Thermal regeneration of diesel particulate monolithic filters. *AICHE J*. 1985;31:753–758.

42. Shah RK, London AL. *Laminar Flow Forced Convection in Ducts: A Sourcebook for Compact Heat Exchanger Analytical Data*. New York: Academic Press, 1978.
43. Koltsakis GC, Stamatelos AM. Modeling thermal regeneration of wall-flow diesel particulate traps. *AICHE J*. 1996;42:1662–1672.
44. Delgado JMPQ. Longitudinal and transverse dispersion in porous media. *Chem Eng Res Des*. 2007;85:1245–1252.
45. Yan YD. Pulse-injection chromatographic determination of the deposition and release rate constants of colloidal particles in porous media. *Langmuir*. 1996;12:3383–3388.
46. Hayes RE, Kolaczkowski ST. A study of Nusselt and Sherwood numbers in a monolith reactor. *Catal Today*. 1999;47:295–303.
47. Hayes RE, Kolaczkowski ST, Li PKC, Awdry S. Evaluating the effective diffusivity of methane in the washcoat of honeycomb monolith. *Appl Catal B: Environ*. 2000;25:93–104.
48. Dudukovic MP, Kulkami MS. Dynamics of gas phase and solid phase reactions in fixed bed reactors. *Chem Eng Sci*. 1996;51:3083–3088.
49. Oh SH, Cavendish JC. Transients of monolithic catalytic convertors: response to step changes in feedstream temperature as related to controlling automobile emissions. *Ind Eng Chem Prod Res Dev*. 1982;21:29–37.
50. Yakhnin V, Menzinger M. High-Temperature transients in catalytic fixed-bed reactors. *Rev Chem Eng*. 2004;20:175–225.

Manuscript received Dec. 30, 2009, and revision received Mar. 22, 2010.